Electronic Supplementary Material (ESI) for ChemComm.

Supporting Information

Visualizing molecular deformation in fibrin networks under tensile loading *via* FLIM-FRET

Mohammadhasan Hedayati,[†a] Yuan-I Chen,[†a] Justin R. Houser,[a] Yujen Wang,[a] Sajjad Norouzi,[a] Hsin-Chih Yeh, [a,b] Sapun H. Parekh *[a]

a. Biomedical Engineering, University of Texas at Austin, Austin, TX, USA.
b. Texas Materials Institute, University of Texas at Austin, Austin, TX, USA.

[†] These authors contributed equally to this work.

* Correspondence should be sent to: sparekh@utexas.edu

Materials:

Human plasma fibrinogen (FIB 3) and human α-thrombin were purchased from Enzyme Research Laboratories. Alexa Fluor 568 NHS ester was purchased from Thermo Fisher Scientific. 3-[methoxy(polyethyleneoxy)6-9]propyltrimethoxy silane was purchased from Gelest. Centri-Sep 20 columns were purchased from Princeton Separations. Atto 488 NHS ester, Tricine, NaCl, $CaCl_2$, and Tween 20 were purchased from Sigma-Aldrich.

Fibrinogen double-labeling:

3 µL of Alexa 568 NHS-ester fluorophore (as acceptor) with a concentration of 15 mM was added to 50 µL of human plasma FIB at 5 mg ml^{-1} in PBS buffer and incubated for 20 min with gentle mixing. For the second labeling step, 1.7 µL of Atto 488 NHS-ester fluorophore (as donor) with a concentration of 10 mM was added to the solution and incubated for 90 min with gentle mixing to conjugate fluorophores to FIB. The resulting FIB-fluorophore conjugate was separated from unbound fluorophores by Centri-Sep columns according to the manufacturer's instructions to render double-labeled FIB (DL-FIB). The degree of labeling (average dye to protein concentration ratio) was determined by using a NanoDrop 2000c (ThermoFisher Scientific) spectrophotometer to measure fluorophore absorption and the protein absorbance at 280 nm, corrected for both fluorophores. The degree of labeling was determined to be 2.5 ± 0.3 and 8.6 ± 0.5 for donor and acceptor, respectively which corresponds to acceptor : donor labeling ratio of 3.4 : 1. To identify the amino acids potentially targeted by the conjugation method, a structural analysis was conducted using the molecular visualization software Pymol on fibrinogen 3GHG model (Fig. S1). The specific locations of the primary amines targeted by the NHS-ester reaction were highlighted with blue spheres. However, it should be emphasized that not all of these primary amines are accessible for the reaction.

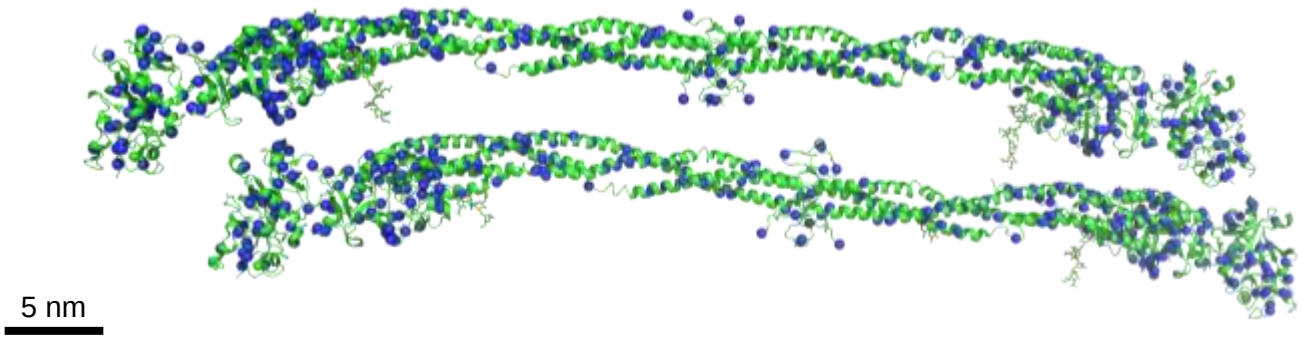

Fig. S1. Targeted primary amines with NHS-ester reaction for dual-labeling of fibrinogen 3GHG model. The blue spheres show the primary amines on fibrinogen. Note the αC domains are not shown as they are disordered and thus do not appear in a crystal structure.

Acceptor photobleaching:

Acceptor photobleaching was performed to measure FRET efficiency of double-labeled fibrin fibers (Fig. S2). Confocal microscope (FV3000, Olympus) with a 60X, 1.1 NA (LUMFLN60XW, Olympus) water dipping objective lens was used to photobleach the acceptor. Fibrin networks were placed directly on the objective, and bleaching was performed for 90 s using 561 nm laser line with 98% intensity to fully photobleach the acceptor. The pinhole on the microscope was always set to 0.75 Airy unit. Images were acquired before and after bleaching and were processed by ImageJ to measure FRET efficiency. FRET efficiency (E) is dependent upon the donor fluorescence intensity, in the presence (I_{DA}) and absence of the acceptor (I_D) and can be measured using Eq. 1.

$$E = 1 - \frac{I_{DA}}{I_D} \quad \text{(Eq.1)}.$$

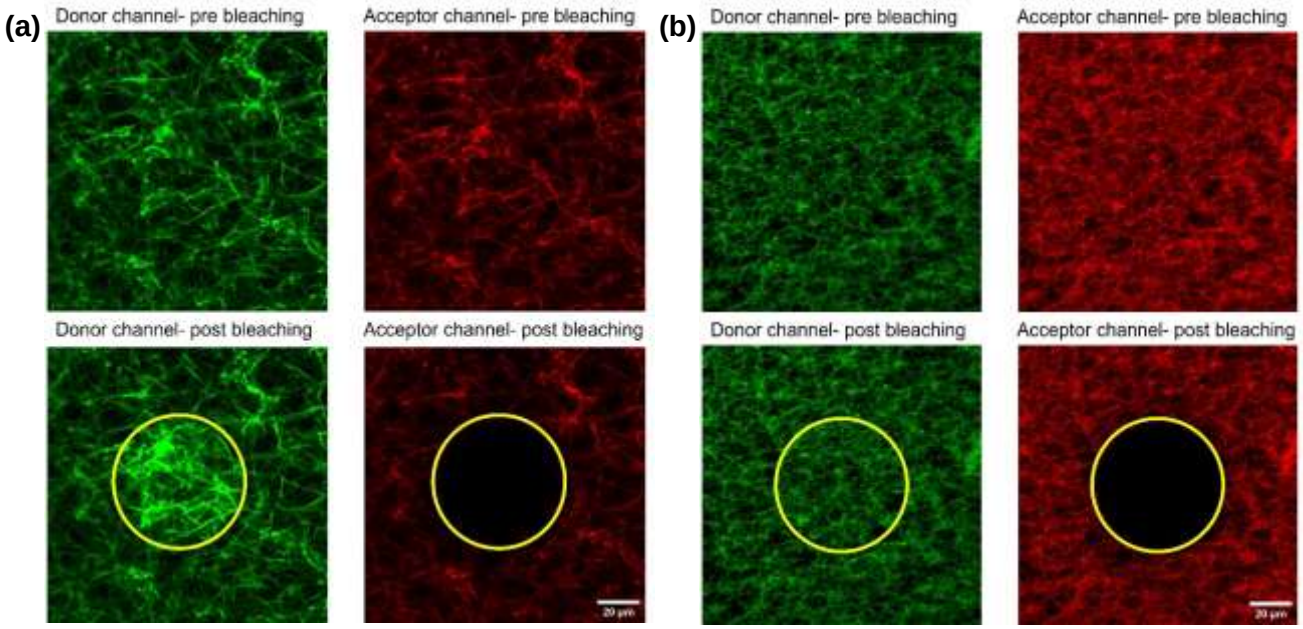

Fig. S2. FRET efficiency measurement by acceptor photobleaching technique for labeled fibrin. (a). Fibrin formed from dual-labeled FIB with Atto 488 and Alexa 568. The circular area demonstrated 45% FRET after photobleaching. (b). Fibrin formed from mixed solution of single-labeled FIB with Atto 488 and single-labeled FIB with Alexa 568. The circular area demonstrated 5% FRET after photobleaching.

Fibrin network preparation:

Fibrin networks were prepared from FIB (5 mg ml^{-1}) with 10% DL-FIB in PBS buffer containing 10 mM Tricine, 150 mM NaCl, 3 mM $CaCl_2$, and 0.005% Tween 20 at pH 7.4. The FIB solution was mixed with human α-thrombin with the final concentration of 1 U ml^{-1} to obtain a pre-gel fibrin solution. Fibrin networks were formed on a tester-compatible stage which was designed to perform uniaxial tensile

stress while imaging with confocal microscopy and FLIM. This stage was designed to hold three coverslips together to allow the formation of fibrin. The first two coverslips (24 × 60 mm^2) act as a support which fibrin sticks firmly from two ends. The third coverslip (24 × 60 mm^2) at the bottom of the other two coverslips is modified with PEG to minimize fibrin attachment and acts as a support. Pre-gel fibrin solution was applied on a defined region on the coverslips (Fig. S3) by a hydrophobic marker which prevents the spreading of the solution. The whole stage was kept in an incubator with 37 °C and 100% humidity for 90 min to form the fibrin network. After fibrin formation, the whole stage was mounted on a microscope-compatible stage and the bottom coverslip was gently removed to perform the tensile loading. To ensure accurate and reliable measurement of tensile strain, we used a calibrated tensile testing setup. The setup consisted of a custom-built instrument capable of applying controlled mechanical strains to the fibrin samples. Uniaxial strain on the network was applied by moving the motorized carriage (Helix Linear, PRA-8S-024) controlled with a microstepping-capable motor controller (Polulu, AMIS 30543). A microstepping ratio of 8:1 was used with a simple Arduino program to control the motor. The setup was calibrated to have ~ 1 µm precision using the microscopy to verify positional accuracy of the stepper motor. The network strain was measured which provided real-time strain data during the experiments. The difference in length (∆L) between the initial length (L_0) and the stretched length (L) of the fibrin network was used to calculate the strain, which was expressed as ∆L/L. The setup was carefully calibrated prior to the experiments to ensure their accuracy. During all strain application, fibrin gels were always kept fully hydrated.

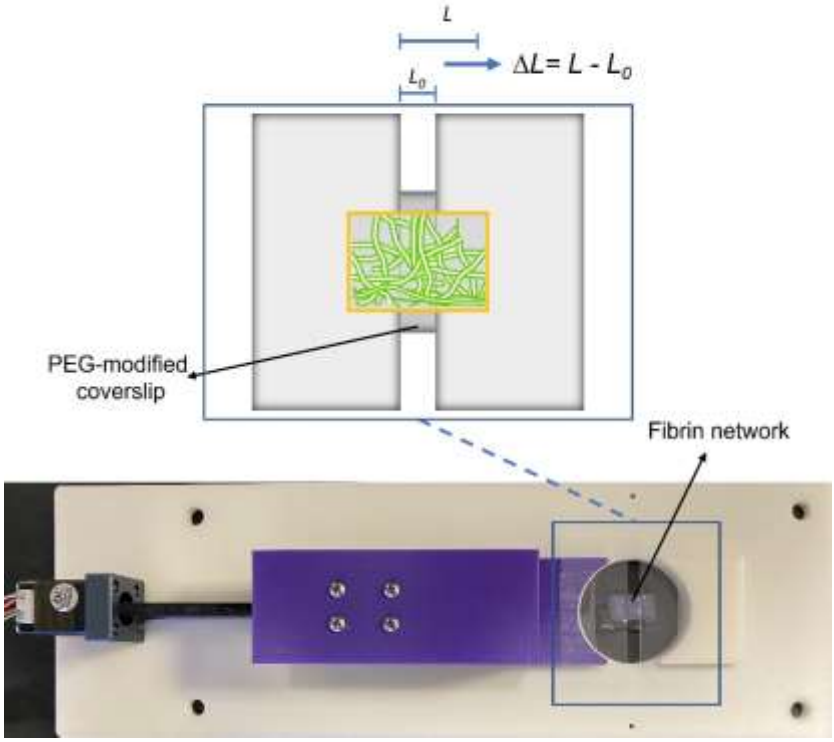

Fig. S3. Imaging-compatible tensile tester to perform tensile loading of fibrin while imaging with confocal microscopy or FLIM using a high-resolution load cell.

FLIM-FRET:

The FLIM system (Alba v5, ISS) was equipped with the diode laser providing 488 nm and a supercontinuum white laser (SuperK EVO, NKT Photonics). All laser lines combined in Alba v5 passed a multi-band dichroic mirror to excite samples. Fluorescence emission light came back along the same path to the multi-band dichroic mirror and went into a detector (SPCM-AQR-15, Perkin Elmer) with 50 nm pinhole. The fluorescence was detected by an avalanche photodiode with corresponding bandpass filter (525/40nm, Semrock). A Nikon inverted microscope with 60x, NA 1.1 water objective (NALUMFLN60XW, Olympus) was used. An ASI XY automatic stage with motorized Z control was equipped in the current setup. The photon counts were acquired with FastFLIM unit to build up the phase histogram. It is necessary to calibrate the FLIM system using a fluorescence lifetime standard before imaging samples. Atto 425, with a reference lifetime of 3.6 ns, was used as the calibration standard in this experiment. The laser repetition period we used was 50 ns, and it was divided into 256 bins. FLIM images were scanned 3 times with dwell time of 0.04 ms/pixel. The data were collected by the confocal scanning system from a 512 x 512-pixel area (50 x 50 μm field of view) before and after uniaxial tension.

The FLIM data was analyzed in digital frequency-domain (DFD) by taking the Fourier transform of the fluorescence decay histogram (Fig. S4). The fluorescence decay histogram of each pixel was plotted as a single point in the phasor plot under corresponding modulation frequency condition. The modulation ratio and phase shift could then be extracted from the point in the phasor plot. With the modulation ratio and phase shift data over multiple modulation frequencies, they were fitted to the fluorescence decay model to obtain the fluorescence lifetime of interest.[1,2] The fibrin fibers with donor only fit to a one-component decay model, resulting in the mean lifetime of 3.22 ns. In dual-labeled fibrin, we expect there are two populations contributing to the fluorescence decay measurements at each pixel: the population of unquenched donor dyes, and the population of quenched donor dyes with FRET. Fixing the 3.22 ns as one lifetime component for unquenched donor dyes, we analyzed the rest of dual-labeled fibrin with bi-exponential decay model.

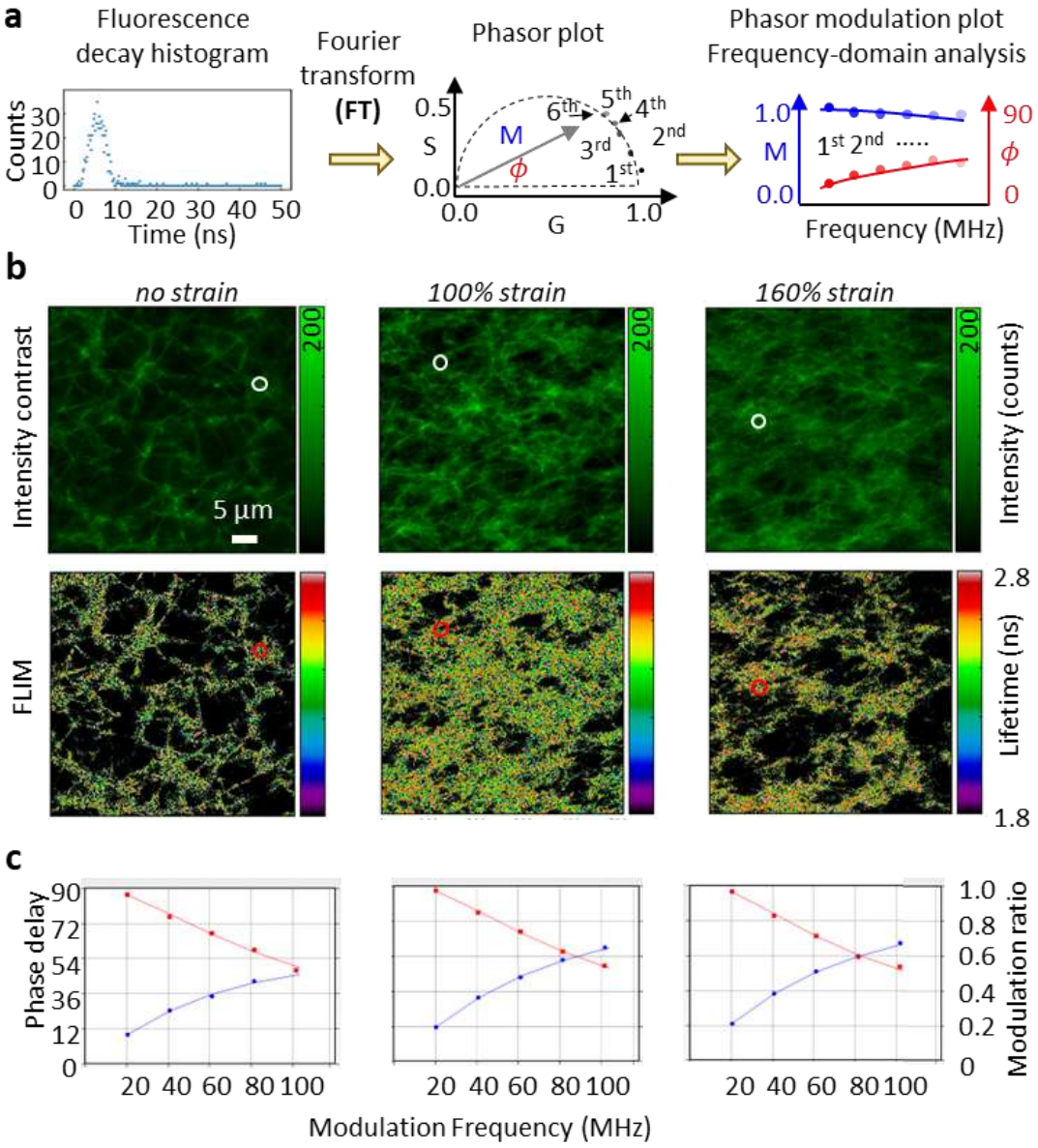

Fig. S4. FLIM analysis in digital frequency-domain (DFD). (a) Schematic of DFD analysis on FLIM data. (b) Intensity and FLIM images obtained from 0%, 100%, and 160% tensile strain. (c) Example data fits at the selected pixels indicated by white circles in (b) show good fitting performance.

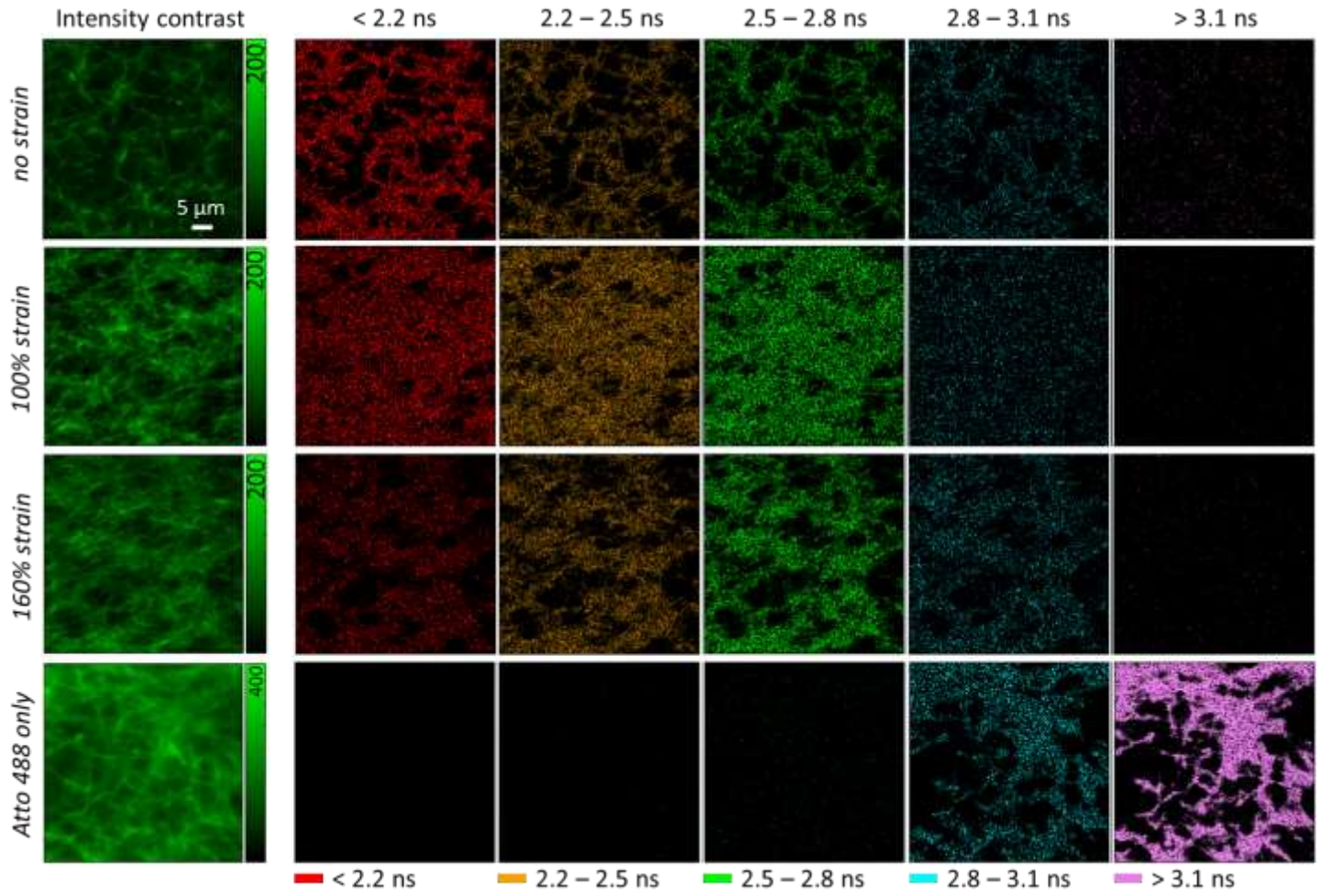

Fig. S5 Intensity contrast and false-color images of fibrin networks obtained from 0%, 100%, 160% tensile strain and with donor only show area-dependent donor lifetime and strain-dependent donor lifetime change.

Orientation analysis:

To assess the local orientation of the fibrin under tensile deformation, we utilized an ImageJ plug-in function, termed OrientationJ.[3] The software determines the local predominant orientation (θ) at each pixel based on the structure tensor. In a 2D image ($f(\boldsymbol{x})$), by definition, the structure tensor ($\boldsymbol{J}(\boldsymbol{x_0})$) is a 2 × 2 matrix describing the distribution of the gradient ($\nabla f(\boldsymbol{x})$, a directional change in the intensity in an image), in a specified neighborhood around a point, $\boldsymbol{x_0}$.

$$\boldsymbol{J}(\boldsymbol{x}_0) = \int w(x - x_0)(\nabla f(x))(\nabla^{\mathrm{T}} f(x))dx_1 dx_2 = \begin{bmatrix} J_{11} & J_{12} \\ J_{21} & J_{22} \end{bmatrix},$$

where $w(\boldsymbol{x}-\boldsymbol{x}_0)$ is a nonnegative isotropic observation window centered at $\boldsymbol{x}_0$. $\boldsymbol{x}_1$ and $\boldsymbol{x}_2$ represent x- and y-axis, respectively. By default, we use cubic spline interpolation to calculate the image gradient. The local predominant orientation, θ, is defined by the following,

$$\theta = \frac{1}{2}\arctan\left(2\frac{J_{12}}{J_{22}-J_{11}}\right),$$

The local predominant orientation is bounded between -π/2 and π/2. Finally, the color-coded orientation map was then displayed. When the fibrin networks are not predominantly oriented, multi-colored orientation map image and the broader distributions of local orientation will be obtained. When the networks become predominantly oriented, single color orientation map image and the narrower distributions of local orientation will be observed.

Integrative analysis of fibrin molecular deformation:

The histogram of orientation and fluorescence lifetime were transformed into the heatmap format. The orientation and lifetime data were binned into multiple groups (cutoffs = ± 70^o, ± 50^o, ± 30^o, ± 10^o for orientation and 2.2, 2.5, 2.8, 3.1 ns for fluorescence lifetime). The number of pixels in the image with the orientation and lifetime lying within certain ranges (e.g., 50^o~70^o orientation and 2.2~2.5 ns lifetime) were then calculated for each condition.

Statistical Analyses:

We assumed a significance level of α = 0.05. The non-significant (n.s.) results were defined as a p-value being greater than 0.05. One star (*) indicated a p-value less than or equal to 0.05 and greater than 0.001. Two stars (**) indicated a p-value less than or equal to 0.01 but greater than 0.001. Three stars (***) indicated a p-value less than or equal to 0.001.

The Kolmogorov-Smirnov (KS) test and the two-sided paired *t*-test were utilized in Fig. 2 and Fig. 3a, respectively, to evaluate the lifetime distribution between different experimental conditions.

References

1 E. Gratton, *J. Biomed. Opt*, 2003, **8**, 381.
2 R. A. Colyer, C. Lee and E. Gratton, *Microsc. Res. Tech.*, 2008, **71**, 201–213.
3 R. Rezakhaniha, A. Agianniotis, J. T. C. Schrauwen, A. Griffa, D. Sage, C. V. C. Bouten, F. N. Van De Vosse, M. Unser and N. Stergiopulos, *Biomech Model Mechanobiol*, 2012, **11**, 461–473.